

SQ-GAN: Semantic Image Communications Using Masked Vector Quantization

Francesco Pezone¹, Sergio Barbarossa², *Fellow IEEE* and Giuseppe Caire³, *Fellow IEEE*,

Abstract—This work introduces Semantically Masked Vector Quantized Generative Adversarial Network (SQ-GAN), a novel approach integrating semantically driven image coding and vector quantization to optimize image compression for semantic/task-oriented communications. The method only acts on source coding and is fully compliant with legacy systems. The semantics is extracted from the image computing its semantic segmentation map using off-the-shelf software. A new specifically developed semantic-conditioned adaptive mask module (SAMM) selectively encodes semantically relevant features of the image. The relevance of the different semantic classes is task-specific, and it is incorporated in the training phase by introducing appropriate weights in the loss function. SQ-GAN outperforms state-of-the-art image compression schemes such as JPEG2000, BPG, and deep-learning based methods across multiple metrics, including perceptual quality and semantic segmentation accuracy on the reconstructed image, at extremely low compression rates. The code is available at <https://github.com/frapez1/SQ-GAN>.

Index Terms—Semantic Communication, VQ-GAN, Data Augmentation, Semantic-Aware Discriminator

I. INTRODUCTION

THE recent surge of intelligent and interconnected devices is leading the transition to new communication paradigms. The upcoming sixth generation (6G) of wireless networks is poised to redefine the communication paradigm by integrating advanced Artificial Intelligence (AI) and networking [1]. One of the most promising advancements in this context is semantic communication, which shifts the focus from universal coding to task-oriented coding, exploiting suitable knowledge representation systems, typically relying on deep neural networks [2], [3], [4], [5], [6]. Recent breakthroughs in deep learning, generative AI, and self-supervised learning have further strengthened the potential of semantic communications. The use of generative AI for next generation networks has been recently proposed in [7], [8], [9]. A key innovation in this domain is the integration of deep generative models that can synthesize, with proper

conditioning, high-fidelity multimedia contents. This capability changes the communication paradigm: instead of transmitting full-resolution data, the transmitter encodes and sends only the most relevant features, which are used at the receiver side to trigger the generative model to reproduce a representation *semantically equivalent* to the transmitted one [10]. The relevance of the features is dictated by the application running on top of the exchange of information. This communication modality enables a drastic reduction in transmission rates, because it takes advantage of application-specific knowledge incorporated in the generative models.

To illustrate this concept, consider a vehicular communication scenario, where one or more autonomous vehicles transmit visual information from their onboard cameras to a roadside unit (RSU) responsible for taking real-time context-aware safety decisions, possibly integrating data from multiple vehicles or RSU sensors. Rather than transmitting full video streams, each transmitter extracts key semantic attributes, such as the presence, shape, and locations of pedestrians, vehicles, traffic signs, and road boundaries, and transmits only compressed feature representations, achieving data rates substantially lower than those needed for conventional image or video encoding. At the receiver side, a generative model reconstructs an application-specific representation, with an accuracy sufficient only to enable the RSU to take rapid decisions within strict latency constraints.

In recent years, deep learning has played a pivotal role in both improving image compression and advancing semantic communication systems [11], [12], [13]. The development of end-to-end learning frameworks enables the joint optimization of the encoding and decoding processes, allowing the overall encoding system to learn a joint source/channel coding (JSCC) technique [14] or to learn efficient representations of semantic content directly from data [15], [11]. Lately, generative models, such as Variational-Autoencoders (VAE), Generative Adversarial Networks (GANs), and Denoising Diffusion Probabilistic Models (DDPM) [16], have been instrumental in improving the quality and efficiency of data representation and transmission [7], [10], [17], [18].

A key step in the integration of generative models within a digital communication scheme, possibly

¹ CNIT - National Inter-University Consortium for Telecommunications, Parma, Italy

² Sapienza University of Rome, Italy

³ Technical University of Berlin, Germany

E-mail: francesco.pezone.ds@gmail.com,

sergio.barbarossa@uniroma1.it, caire@tu-berlin.de

compliant with legacy systems, is to merge generative models and vector quantization to learn discrete latent representations that are both compact and semantically rich [19], [20]. Models like the Vector Quantized VAE (VQ-VAE), the Vector Quantized GAN (VQ-GAN) and the Masked VQ-VAE (MQ-VAE) [21] have already demonstrated remarkable capabilities in image synthesis and compression tasks.

Given this context, in this paper we propose the Semantic Masked VQ-GAN (SQ-GAN) model, a novel approach that merges the strengths of generative models, vector quantization, and semantic segmentation for efficient and semantic-preserving image transmission. We choose the GAN paradigm because it provides a good tradeoff between simplicity and accuracy. In the proposed scheme, semantic information is extracted from the image \mathbf{x} to be transmitted by computing its Semantic Segmentation Map (SSM) \mathbf{s} , using some suitable state-of-the-art (SOTA) algorithm (in our implementation we used INTERN-2.5 [22]). Then, SQ-GAN applies a semantically-guided vector quantization strategy to encode both \mathbf{x} and \mathbf{s} . In particular, SQ-GAN learns a vector quantization codebook from the data and applies a newly designed and trained adaptive selective masking to dynamically adjust the compression rate, ensuring that semantically important features are retained. This is obtained by a specifically designed semantic-conditioned variant of the masked vector quantization introduced in [21] to prioritize semantically significant information, thus reducing redundancy while preserving the relevant semantic content. The new adaptive masking mechanism is trained to select the elements in the latent space tensor that are most significant for the preservation of the image's semantic content. Only these selected elements are then quantized, using vector quantization with the learned codebook. Finally, the decoder part of the scheme is formed by some learned blocks, trained to reconstruct the original image by minimizing an error function that includes the SSM. The key innovations in the proposed SQ-GAN scheme are: (i) a novel GAN-based model that integrates semantic conditioning and compression directly into its architecture, (ii) the Semantic conditioned Adaptive Mask Module (SAMM) that selects and encodes the most semantically relevant features of the input data based on the SSM, (iii) a specifically designed data augmentation technique in the training phase to enhance the semantically relevant classes, and (iv) the inclusion (in training) of a semantic-aware discriminator to force the model to give more importance to the semantically relevant regions over the non-relevant ones.

Before proceeding, some important remarks regarding our method are in order:

i) Since we focus on task-oriented semantic commu-

nication, we assume that the semantic classes used by the state-of-the-art semantic segmentation algorithm are predefined according to the task requirements. Furthermore, the relevance of each class is quantified by weights $w_i \in [0, 1]$ assigned to each i -th class. These weights are incorporated into the loss functions used to train the proposed SQ-GAN. The combination of this task-oriented weighted loss function and the aforementioned task-specific data augmentation during training results in an SQ-GAN model optimized for the target application. For instance, in our numerical examples focused on autonomous driving scenarios, the relevant object classes include pedestrians, cars, traffic lights, and similar entities.

ii) The assumption that the SSM \mathbf{s} is extracted from the raw image \mathbf{x} in real-time at the encoder is fully realistic. For example, in the autonomous driving scenario, there are algorithms able to extract the SSM in real time, see, e.g. [23]. In particular, Tesla has already deployed the technology to analyze raw images and perform semantic segmentation and object detection in their per-camera networks in real time, as reported in [24].

iii) Our scheme treats only source coding (i.e., image compression/reconstruction), unlike several works on semantic communications that have considered a JSCC setting. This makes our approach completely compatible with any underlying legacy network protocol, where source coding/decoding takes place at the application layer and the source-coded bits are transmitted to the destination via some standard protocol stack (e.g., a 3GPP wireless network).

This work is organized as follows. Section II introduces the scope and general overview of the proposed architecture. Section III introduces in more detail the different parts of the proposed SQ-GAN model. Section IV discusses the training method with data augmentation for the enhancement of semantically relevant classes and the semantic-aware discriminator employed to optimize the SQ-GAN. Finally, Section V presents numerical experiments demonstrating the effectiveness of SQ-GAN compared to state-of-the-art (SOTA) image compression techniques such as JPEG2000, Better Portable Graphics (BPG) and the GAN based High-Fidelity Generative Image Compression (HiFiC) [12] and Fidelity-Controllable extreme image Compression (FCC) [13].

II. PROBLEM STATEMENT AND GENERAL ARCHITECTURE

The objective of this work is to develop an image encoder that efficiently compresses an image \mathbf{x} , while preserving its semantic content as much as possible, even at extremely high compression rates. In this work, the semantic content is identified with the SSM \mathbf{s} ,

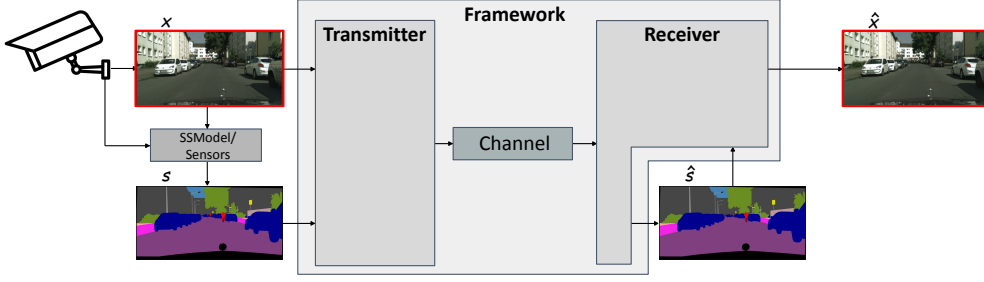


Figure 1: Schematic representation of the overall coding/decoding scheme.

extracted in real-time from \mathbf{x} using a SOTA Semantic Segmentation Model (SSModel) [22] with pre-defined semantic classes that depend on the task at hand, as explained in Section I.

As schematically shown in Fig. 1, our encoding scheme extracts \mathbf{s} from \mathbf{x} and then jointly encodes \mathbf{x} and \mathbf{s} . At the decoder, \mathbf{x} and \mathbf{s} are reconstructed as $\hat{\mathbf{x}}$ and $\hat{\mathbf{s}}$, respectively. In some sense, this approach is akin layered source coding, where \mathbf{s} can be seen as the “fundamental layer” and \mathbf{x} is the refinement. The goal is to achieve good reconstruction performance (with respect to distortion metrics to be defined later) at a low overall coding rate, in terms of Bits Per Pixel (BPP). The key result of our work is to show that, even though we transmit two images, namely \mathbf{x} and \mathbf{x} instead of just \mathbf{x} , we achieve a significantly better trade-off between the overall coding rate and various metric for semantic distortion with respect to SOTA schemes (including data-driven approaches).

By jointly encoding and decoding \mathbf{x} and \mathbf{s} , and incorporating the reconstruction of $\hat{\mathbf{s}}$ in the decoder, it is possible to directly optimize the preservation of semantic information and assign different importance to different semantic classes during the training process and use $\hat{\mathbf{s}}$ to condition the reconstruction of $\hat{\mathbf{x}}$. Intuitively, this conditioning “pushes” the decoder to align $\hat{\mathbf{x}}$ with the semantic structure of the original image \mathbf{x} .

The detailed architecture of the proposed SQ-GAN scheme is shown in Fig. 2, where the original image \mathbf{x} and the corresponding original SSM \mathbf{s} are both represented by 3-dimensional tensors. The image \mathbf{x} is a tensor of size $3 \times H \times W$, where 3 refers to the RGB channels, H is the height and W is the width of the frame (in pixels). In this work, we have used images of size $H = 256$ and $W = 512$. The SSM \mathbf{s} is a tensor of size $n_c \times H \times W$, where n_c is the number of semantic classes, H is the height and W is the width of the frame. Each n_c -dimensional vector in pixel position (h, w) represents the 1-hot encoding of the corresponding semantic class of that pixel. This representation is quite standard and has proven to be convenient in a large number of works on semantic-conditioned image generation.

The compression and reconstruction of the image \mathbf{x} and of its SSM \mathbf{s} is accomplished by two parallel (and mutually interacting) pipelines. We use apex/subscripts \mathbf{x} and \mathbf{s} to indicate blocks of the specific pipeline. Looking at the transmitter side, the bottom pipeline (in beige) reports the encoder of the SSM, whereas the top pipeline (in green) reports the image encoding process, which is conditioned to the SSM. The semantic encoder E_s takes as input the original SSM \mathbf{s} and outputs the latent tensor $\mathbf{z}^s = E_s(\mathbf{s})$ of shape $C \times H_{16} \times W_{16}$ where $C = 256$, $H_{16} = \frac{H}{16}$ and $W_{16} = \frac{W}{16}$. In parallel, the image encoding pipeline first extracts the latent representations of \mathbf{x} and \mathbf{s} , using two pre-trained DNNs, namely the InputNet_x for \mathbf{x} and the proposed Semantic Positional Embedding (SemPE) for \mathbf{s} . These latent representations are added together as $\mathbf{h}(\mathbf{x}, \mathbf{s}) = \text{InputNet}_x(\mathbf{x}) + \text{SemPE}(\mathbf{s})$ and sent to the encoder that produces the latent tensor $\mathbf{z}^x = E_x(\mathbf{h}(\mathbf{x}, \mathbf{s}))$, having the same shape as \mathbf{z}^s . Both tensors \mathbf{z}^x and \mathbf{z}^s are composed of $K = H_{16} \times W_{16}$ latent vectors \mathbf{z}_k^x and \mathbf{z}_k^s in C dimensions.

The tensors \mathbf{z}^x and \mathbf{z}^s are then sent to the corresponding Semantic conditioned Adaptive Mask Module (SAMM) blocks, which select the most semantically relevant latent vectors. The SAMM blocks play a key role in reducing the transmission rate, while preserving the most relevant information. The number of selected latent vectors depends on a masking fraction variable m^x , or m^s , that can be set as a parameter. Hence, only $N_x = \lfloor m^x K \rfloor$ and $N_s = \lfloor m^s K \rfloor$ selected latent vectors from \mathbf{z}^x and \mathbf{z}^s are quantized, respectively.

Vector quantization (VQ) is applied separately to each selected vector, where the quantization codebook is formed by J learnable C -dimensional vectors (quantization codewords) denoted by \mathbf{e}_j^x and \mathbf{e}_j^s , $j \in \{1, \dots, J\}$, respectively. Therefore, each quantized latent vector is identified by a binary index of $\log_2 J$ bits. In this work we chose $J = 1024$ and the ℓ_2 distance as the quantization metric (more in Section III-D). The quantized latent tensors are denoted by \mathbf{z}_q^x and \mathbf{z}_q^s , respectively. The list of quantization indices \mathbf{e}_j^x and \mathbf{e}_j^s , including the positions

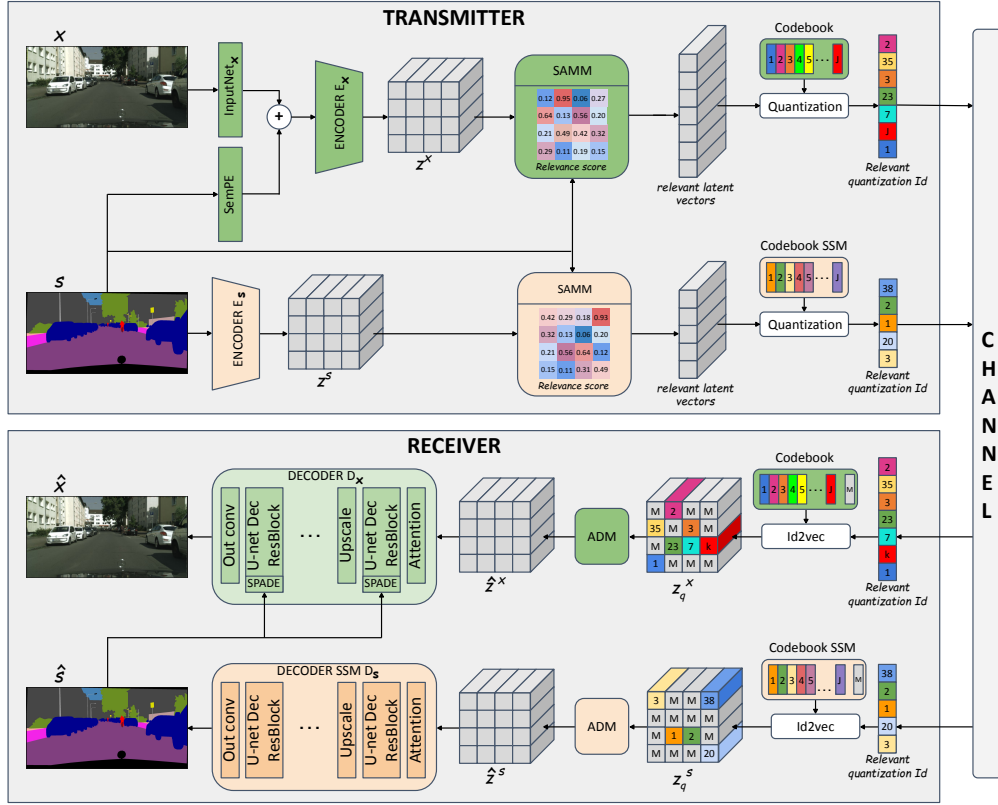


Figure 2: Encoder and decoder detailed structure of the proposed SQ-GAN scheme. The “channel” here may represent transmission or storage, depending on the application.

of the discarded non-relevant indices, are binary encoded and form the binary encoded stream to be transmitted.

At the receiver side, the binary stream is decoded and formatted into the latent space tensors \mathbf{z}_q^x and \mathbf{z}_q^s . Following a similar procedure as in [21], the latent tensors contain the quantized vectors in the positions where these vectors were selected and effectively quantized, and a “placeholder” codeword M_x or M_s in the masked-out positions. These placeholder codewords are not necessarily all-zero vectors, and can be learned in the training phase in order to facilitate reconstruction. These latent space tensors are then processed by the Adaptive De-Mask Module (ADM) module to produce the reconstructed latent space tensors $\hat{\mathbf{z}}^x$ and $\hat{\mathbf{z}}^s$, respectively.

Finally, the latent tensor $\hat{\mathbf{z}}^s$ is processed by the decoder D_s to produce the reconstructed \hat{s} and the latent tensor $\hat{\mathbf{z}}^x$ is processed by the decoder D_x to produce the reconstructed \hat{x} with conditioning provided by \hat{s} .

The details of the blocks appearing in Fig. 2 and the overall training method will be illustrated in the next section. In particular, it is important to clarify that the training of the proposed SQ-GAN is performed via an adversarial approach based on two discriminators. However, in Fig. 2 only the structure of the generator

is represented. In fact, the generator is eventually the trained model deployed and used at the run-time, while the discriminators play a role only in the training phase.

III. MASKED SEMANTIC VQ-GAN (SQ-GAN)

This section describes in detail the individual blocks of the proposed SQ-GAN architecture.

A. Semantic Encoder

The encoder E_s maps the $n_c \times H \times W$ SSM s to a latent tensor $\mathbf{z}^s = E_s(s)$ with shape $C \times H_{16} \times W_{16}$, where $C = 256$ is the hyperparameter representing the number of channels and H_{16} and W_{16} are the height and width. E_s is formed by a repeated sequence of two Residual Blocks (ResBlocks) [25] and one down-scaling layer, which will be referred to as ResBlock-Down. The average pooling down-scaling layer halves the height H and width W of the SSM. By applying 4 cascaded stages of ResBlock-Down, the final latent tensor has shape $H_{16} \times W_{16}$. We decided to use 4 ResBlock-Downs stages based on an extensive ablation study (not reported here because of space limitation), where this choice emerged as the best balance between compression and reconstruction accuracy. The output of

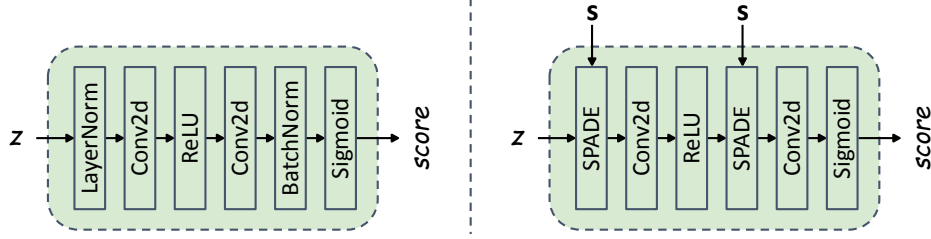


Figure 3: Architectural diagram of the AMM as in [21] (left), and the proposed SAMM employing the SPADE layer to introduce the SSM conditioning (right).

the last ResBlock-Down is processed by the final multi-head self-attention layer of the encoder as in [21].

B. Image Encoder

The image encoder E_x maps the image x to the latent representation z^x of shape $C \times H_{16} \times W_{16}$, using the conditioning provided by s . E_x has the same structure as E_s . The main difference lies in the conditioning process. In fact, not all the parts of the image x have the same semantic meaning and relevance: for example, in assisted driving applications, pedestrians are more important than the sky.

To help the encoder E_x assign different importance to different parts, the image x is modified before encoding. The proposed method draws inspiration from the version of the Positional Embedding (PE) introduced by Dosovitskiy et al. for transformer networks in vision tasks [26]. That scheme divides the image into 16×16 patches and assigns a specific PE vector to each patch to allow the transformer to correctly interpret the relative positions of the patches in the frame. In our case, PE as proposed in [26] is not needed since, unlike transformer architectures, the spatial correlations are preserved in convolution-based architectures. However, the idea of assigning different weights to different semantic regions of the image is used to improve the overall performance. Hence, we propose a variation of PE, referred to as SemPE, whose goal is to provide the encoder E_x with a suitable transformation of s that can be used to influence the feature extraction process. SemPE processes s using a two layer Convolutional Neural Network (CNN) designed to take into account the semantic classes of adjacent pixels. In parallel, the image x is processed by a one-layer CNN called InputNet $_x$. The outputs of both SemPE and CNN are tensors of shape $128 \times H \times W$. Then, as in the classical PE, the input of the encoder is formed by the elementwise sum $h(x, s) = \text{InputNet}_x(x) + \text{SemPE}(s)$. This is then processed by the encoder E_x to produce the latent tensor $z^x = E_x(h(x, s))$ of shape $C \times H_{16} \times W_{16}$.

C. Semantically Conditioned Adaptive Mask Module

The latent tensors z^x and z^s can be interpreted as collections of $K = H_{16}W_{16}$ vectors of dimension C . The next step is to select the most relevant $N_x = \lfloor m_x K \rfloor$ vectors in z^x and $N_s = \lfloor m_s K \rfloor$ vectors in z^s , where the relevance masking fraction $m_x \in (0, 1]$ and $m_s \in (0, 1]$ are design parameters. This selection is performed by the SAMM blocks, which we illustrate next. We only refer to the latent tensor z^x , as its application to the pipeline is similar.

SAMM is a variation of the Adaptive Mask Module (AMM) introduced in [21]. The key idea consists of assigning to each of the K latent vectors a relevance score and then select the N_x vectors with the highest score. In the proposed SAMM, the relevance score is conditioned on the SSM s and the masking fraction m_x can be adjusted dynamically. This allows the network to use the same weights to compress images at different levels of compression. The architecture of the conventional AMM and the new SAMM is shown in Fig. 3. While the classic AMM, on the left, is more suitable for general purpose applications, the SAMM on the right is designed to take into account the semantic class of the different regions of the image. The new SAMM enforces this conditioning thanks to the Spatially-Adaptive Normalization (SPADE) normalization layer [27]. The key advantage of this semantic conditioning is its ability to identify and prioritize the accurate representation of the regions of the image corresponding to the important semantic classes without requiring additional trainable parameters. Without the masking driven by the SSM, the encoding model would have required many more parameters to learn the features of relevant objects and correctly use this information as input of the AMM.

SAMM takes as input the latent tensor z^x and the SSM s and outputs a relevance score $\alpha_k^x \in [0, 1]$ for each latent vector z_k^x . The final step involves the multiplication of the selected latent vectors by their respective relevance scores. This is done to allow backpropagation to flow through SAMM and train its parameters, as discussed in [21].

D. Quantization and Compression

After selecting the N_x latent vectors having the highest score, the selected vectors are vector-quantized, while the not relevant $K - N_x$ latent vectors are just dropped. The vector quantization process follows the same steps as the classic MQ-VAE [21]. A learnable codebook $\mathcal{C}_x = \{\mathbf{e}_j^x : j = 0, \dots, J - 1\}$ is used, where in this application we found convenient to use $J = 1024$ codewords of dimension $C = 256$. For each selected score-scaled relevant vector $\mathbf{z}_k^x = \alpha_k^x \mathbf{z}_k^x$, the codeword at minimum distance is found, i.e., the codeword index j is selected such that

$$j = \underset{i \in \{1, \dots, J\}}{\operatorname{argmin}} \|\mathbf{z}_k^x - \mathbf{e}_i^x\|^2, \quad (1)$$

The sequence of quantization indices is then binary encoded using entropy coding. Every latent vector selected for quantization is located in some position in a $H_{16} \times W_{16}$ shaped array. Therefore, the quantized array is formed by N_x positions containing quantization indices (i.e., integers from 0 to $J - 1$ selected as in (1)) and $K - N_x$ “empty” positions corresponding to the discarded vectors. We assign to all discarded positions an additional special index (conventionally denoted as -1), so that we can interpret the quantized array as a discrete information source over an alphabet of size $J + 1 = 1025$. The index -1 appears with probability $1 - m_x$, while the other indices from 0 to $J - 1$ appear with probabilities β_j such that $\sum_{j=0}^{J-1} \beta_j = m_x$. In general, these probabilities are unknown and depend on the specific image \mathbf{x} to be encoded. However, using the fact that entropy is maximized by the uniform probability distribution, we obtain an upper bound to the length of the entropy-coded binary sequence by assuming $\beta_j = \frac{m_x}{J}$. Therefore, the entropy coding rate for the index sequence is upper-bounded by:

$$R_x = h_2(m_x) + m_x \log_2(J),$$

where $h_2(p) = -(1 - p) \log_2(1 - p) - p \log_2(p)$ is the binary entropy function. Since the index sequence length is K , the number of bits necessary to represent such a sequence is therefore upper-bounded by $B_x = R_x K$. Notice that this is indeed a brute-force bound, and in fact any suitable more refined compression scheme (e.g., using arithmetic coding coupled with Krichevsky-Trofimov probability sequential estimation [28]) would achieve a lower rate. However, in this work this value is further approximated. To maintain a linear relationship between the number of bits and the number of relevant latent vectors, the condition $h_2(p) \leq 1$ is used. By substituting $h_2(p) = 1$, the final number of bits is expressed as follows:

$$B_x = K(1 + m_x \log_2(J)).$$

As will be pointed out in Section V, even under this coarse upper bound, SQ-GAN consistently outperforms competing SOTA image compression algorithms. By considering the same approach for the N_s relevant vectors in \mathbf{z}_s , $J = 1024$, and normalizing by the total number of pixels HW , we can express the overall coding rate in BPP as a function of m_x and m_s as:¹

$$\text{BPP} = \frac{B_x + B_s}{HW} = \frac{1}{256} [10(m_x + m_s) + 2], \quad (2)$$

where $K/(HW) = H_{16}W_{16}/(HW) = 1/256$. Notice that this formulation of the BPP considers the contribution of both the image and its SSM. Therefore, the BPP given above is fully consistent with the definition of source coding rate in image coding (coded bits per image pixel).

E. Tensor Reconstruction and Adaptive De-Masking Module

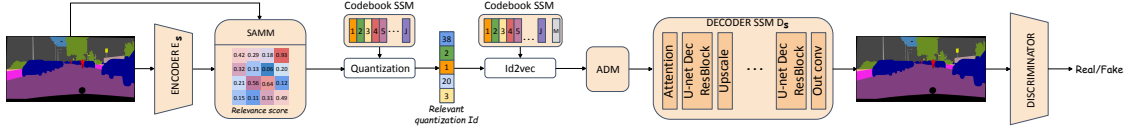
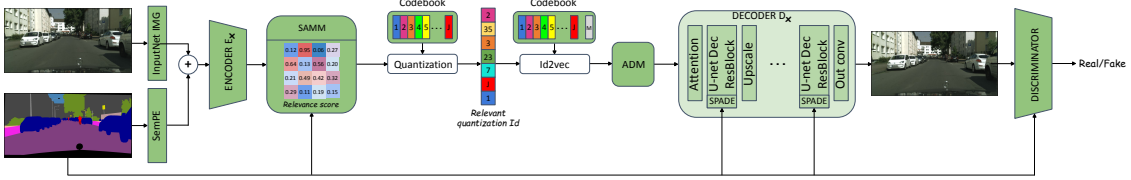
At the receiver, the codebooks \mathcal{C}_x and \mathcal{C}_s are stored in the decoder. The bit stream is decoded and the array of quantization indices is retrieved. Then, a tensor of shape $C \times H_{16} \times W_{16}$ is obtained by placing quantization codewords \mathbf{e}_j^x in correspondence of indices $j \in \{0, \dots, J - 1\}$ and a placeholder codeword denoted as \mathbf{M}_x in correspondence of all indices equal to -1 (i.e., in the position of the discarded latent space vectors). A similar operation is done for the s pipeline, where the placeholder is denoted by \mathbf{M}_s . The placeholders are also learned in the training phase.

The resulting tensor is processed by the Adaptive De-Masking Module (ADM). This step is similar to what was introduced in MQ-VAE [21] and makes use of a direction-constrained self-attention mechanism to gradually let the information flow from the relevant \mathbf{e}_j^x to the non-relevant placeholder \mathbf{M}_x . This can be interpreted as a sort of non-linear “interpolation” of the latent space tensor in the discarded positions. The output $\hat{\mathbf{z}}^x$ of the ADM is then used as the input of the decoder D_x . Similarly, the output $\hat{\mathbf{z}}^s$ of the ADM in the s pipeline forms the input of the decoder D_s . At this point, the flows for the two pipelines for x and for s diverge again, as described in the next two subsections.

F. Semantic Decoder

The structure of the decoder D_s is similar to a mirrored version of the encoder E_s . The first input layer is composed of the multi-head self-attention layer, after which the series of ResBlock-Ups is placed. Every ResBlock-Up is composed of two consecutive ResBlocks

¹In our results, when referring to BPP, it is generally intended this total BPP, unless otherwise specified.

Figure 4: Schematic representation of the semantic generator network G_s training pipeline.Figure 5: Schematic representation of the image generator network G_x training pipeline.

and one up-scaling layer. The up-scaling is performed by copying the value of one element in the corresponding up-scaled 2×2 patch. The goal is to gradually transform the latent tensor \hat{z}^s from a shape of $C \times H_{16} \times W_{16}$ back to the original shape of $n_c \times H \times W$, the same as the SSM s . This decoding and up-scaling process is completed by using four consecutive ResBlock-Ups. The final reconstructed SSM \hat{s} is obtained by the standard practice of applying the argmax operator to assign each pixel to a specific semantic class [29]. The reconstructed SSM \hat{s} can now be used to condition the reconstruction \hat{x} of the image x , as described next.

G. Image Decoder

The reconstruction of x is obtained by applying the decoder D_x to \hat{z}^x and to the reconstructed SSM \hat{s} . This decoder has a structure similar to the mirrored version of the encoder E_x , with some key conceptual differences. The input multi-head self-attention layer has the same structure as the one used in the semantic decoder. The sequence of four consecutive ResBlock-Up is modified to incorporate the conditioning via the SSM. The modifications focus on the normalization layers within the ResBlocks, replacing every normalization layer with the SPADE layer. This new layer is responsible for enforcing the structure of the SSM during the decoding phase [27].

IV. TRAINING AND INFERENCE

So far we have provided a structural and functional description of the blocks that compose the encoder and the decoder, as shown in Fig. 2. In this section, we illustrate the training phase of all these blocks, considering both image and SSM pipelines. We recall that the GANs rely on the interplay between a generator and a discriminator. The generator G_s of the semantic part is coupled with the corresponding discriminator, denoted as D_{disc}^s , while the image generator G_x is

paired to the corresponding discriminator D_{disc}^x . The discriminator is a neural network that receives either an image or the SSM as input and assesses its authenticity by distinguishing between real and generated samples. It is used exclusively during training to guide the generator, providing feedback on how realistic its outputs are. This feedback enables the generator to progressively improve the quality and realism of the data it produces. The training scheme for G_s is shown in Fig. 4, while that for G_x is shown in Fig. 5. At runtime (i.e., when the trained model is applied to a generic image for compression and reconstruction), the discriminators play no role.

The two pipelines are intended to reconstruct objects in distinct domains – the image domain and the SSM domain – each requiring different loss functions. After intensive numerical experimentation, we realized that training the entire network as a monolithic entity (i.e., of both pipelines coupled together as in Fig. 2) is not efficient. Additionally, it is useful to consider the masking fractions m_s and m_x as variable rather than fixed as in [21]. This allows SQ-GAN to compress images and SSMs at various compression levels, but also increases the training complexity. Hence, to effectively train SQ-GAN, we devised a multi-step approach consisting of three stages: (i) train G_s using the original s , (ii) train G_x with the original x and s and (iii) fine-tune the entire network, denoted by G , using the original x , original s , and the reconstructed \hat{s} by freezing G_s 's parameters and only fine-tuning G_x 's parameters. Initially training G_s ensures that the SSM is accurately reconstructed independently of the rest. At the same time, training G_x with the original x and s allows learning the conditional dependencies required for image reconstruction based on a reliable SSM. However, since the decoder part in G_x is later required to be conditioned by the reconstructed \hat{s} rather than the original s , the fine-tuning step is crucial to adapt G_x to mitigate the imperfections of \hat{s} that are not present in s .

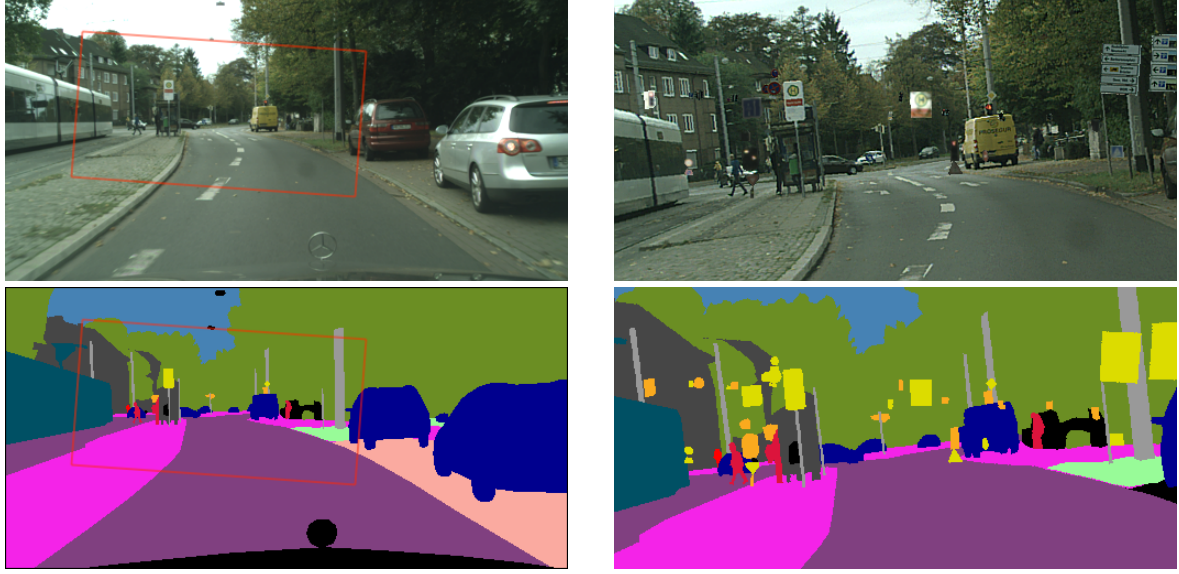


Figure 6: Effect of combined data augmentation techniques, including rotation, cropping and the proposed semantic relevant classes enhancement. On the left, the original image and SSM and on the right the resulting augmented version.

In addition to the multi-step training approach, another crucial challenge is the identification and preservation of semantically relevant information. To address this problem, the training process has been further improved by proposing and incorporating a data augmentation step, adding semantically relevant classes, and a *semantic-aware discriminator network*. The idea is to emphasize the importance of semantically relevant classes. For example, in our numerical experiment we focused on dashboard camera views for assisted driving applications, where the semantic classes of interest are (for example) "traffic signs", "traffic lights", and "pedestrians". These objects typically occupy a small portion of the frame and are not always present in every frame. In contrast, non-relevant classes such as "sky", "vegetation", and "street", appear much more frequently and occupy a large portion of the images. Therefore, Data augmentation is used to ensure that frequent but task-irrelevant semantic classes do not dominate the training process.

This section is organized as follows. Section IV-A will present the data augmentation process as well as the proposed method for enhancing semantically relevant classes. Section IV-B will focus on the training of G_s , while Section IV-C will focus on the training of G_x with the introduction of the proposed semantic-aware discriminator. Finally, Section IV-D will focus on the final fine-tuning process. The dataset used for training is the Cityscapes dataset [30] composed of 2975 pairs of images and associated SSMs.

A. Data Augmentation

This section introduces a novel data augmentation technique aimed at addressing the issue of underrepresented but semantically important classes in datasets. This new data augmentation technique is fundamentally different from previously proposed methods (e.g., [31], [32]). These approaches often focus on swapping existing objects – for example, replacing a "turn left" sign with a "stop" sign – or employ complex Neural Network (NN) architectures to introduce new objects into images. These approaches can lead to increased computational costs or fail to adequately address the under-representation of critical classes. In contrast, the proposed technique is straightforward, efficient, and fast.

For the sake of illustration, let us focus on data augmentation to address the under-representation of "traffic signs" and "traffic lights". The process is based on the use of mini-batches of pairs (x, s) . For each image in a mini-batch, the SSM is used to identify all instances of "traffic signs" and "traffic lights" present in that image. Then, each image and its corresponding SSM is augmented by adding more instances of these critical classes. This is achieved by copying "traffic signs" and "traffic lights" from other images within the same mini-batch and pasting them into the current image and SSM. By increasing the presence of these objects, the model will be more exposed to them during training.

The process begins by collecting all "traffic signs" and "traffic lights" from the images and SSMs in the current mini-batch. For each image in the mini-batch,

a random number n between 0 and 25 is selected, representing the number of objects to add. Then, n objects are randomly selected from the collected set and carefully inserted into the image and its SSM. The placement is carried out in such a way as to avoid overlapping with existing instances of the same class or other semantically relevant classes. An example of an augmented pair (\mathbf{x}, \mathbf{s}) is represented in Fig. 6 with the original pair on the left and the data augmented version on the right. Other classic data augmentation techniques like cropping, rotation and color correction are also applied. However, it is interesting to notice the increase in "traffic signs" (yellow), and "traffic lights" (orange) in the augmented \mathbf{x} and \mathbf{s} .

B. Training G_s

The training of the sub-network G_s is implemented as depicted in Fig. 4, based on an adversarial approach VQ-GANs applied to the training set with data augmentation. The input and output tensors \mathbf{s} and $\hat{\mathbf{s}}$ of G_s have a shape $n_c \times H \times W$. We considered the following loss function:

$$\begin{aligned} \mathcal{L}_{\text{SQ-GAN}}^s &= \mathcal{L}_{\text{WCE}} + \\ &+ \lambda_{\text{GAN}} [\log D_{\text{disc}}^s(\mathbf{s}) + \log (1 - D_{\text{disc}}^s(G_s(\mathbf{s})))] \\ &+ \lambda_{\text{vq}} \|\text{sg}[\mathbf{z}'^s] - \mathbf{z}_q^s\|_2^2 + \lambda_{\text{commit}} \|\mathbf{z}'^s - \text{sg}[\mathbf{z}_q^s]\|_2^2 \\ &:= \mathcal{L}_{\text{WCE}} + \lambda_{\text{GAN}} \mathcal{L}_{\text{GAN}} + \lambda_{\text{vq}} \mathcal{L}_{\text{vq}} + \lambda_{\text{commit}} \mathcal{L}_{\text{commit}} \end{aligned} \quad (3)$$

where the λ 's are hyperparameters that control the strength of each term. The last three terms in (3) are the same as in [20] for the conventional VQ-GAN. More specifically, \mathcal{L}_{GAN} is the term responsible for adversarial training. This term encourages the generator to produce outputs that are indistinguishable from real semantic maps by penalizing the generator if the discriminator can differentiate between the real and generated images. The structure of the discriminator D_{disc}^s is that of a neural network as described in [33]. This is composed of a convolutional layer, batch normalization layer and a leaky ReLU [34] repeated 3 times and followed by the last convolutional layer that maps the output to a single number. This value is the output of the discriminator used to classify the SSM as real or fake. As a result, \mathcal{L}_{GAN} improves the overall quality of the generated semantic reconstructions by guiding the model toward realistic results. The \mathcal{L}_{vq} term is responsible for training the codebook used in the quantization process. It utilizes the $\text{sg}[\cdot]$, which is the stop-gradient operator. This operator prevents the gradients from being back-propagated to the encoder during training. By blocking the backpropagation, the encoder's parameters are not updated, and the codebook is encouraged to adjust its codewords to better match the output of the encoder. The $\mathcal{L}_{\text{commit}}$ term ensures that the encoder does not overfit

to only a small subset of the codebook entries. This is obtained by penalizing the difference between the encoder's output \mathbf{z}' and the quantized codebook entry $\text{sg}[\mathbf{z}_q]$, thus promoting the encoder to use a more diverse set of codebook entries. As a result, the generalization and stability of the training process are improved while ensuring that the codebook entries are not updated during the training of the encoder.

The first term of the loss function in Eq. (3) is a novelty introduced in this work and consists of the weighted cross-entropy \mathcal{L}_{WCE} defined as:

$$\mathcal{L}_{\text{WCE}}(\mathbf{s}, \hat{\mathbf{s}}) = - \sum_{(h,w)} \mathbf{w}_{\mathbf{s}(h,w)} \mathbf{s}(h,w) \log (\mathbf{s}(h,w) \cdot \hat{\mathbf{s}}(h,w)),$$

where $\mathbf{s}(h,w)$ and $\hat{\mathbf{s}}(h,w)$ denote the one-hot encoded vectors at pixel location (h,w) in \mathbf{s} and $\hat{\mathbf{s}}$, respectively, and $\mathbf{w}_{\mathbf{s}(h,w)} \geq 0$ is the weight associated with the semantic class in that pixel. This choice is motivated by the nature of the SSM, which is a pixel-wise classification map where each pixel belongs to a specific semantic class. The weights are assigned to emphasize the importance of semantically relevant classes over nonrelevant ones, encouraging the model to focus more on reconstructing the critical classes. Specifically, in the training of the model used in our numerical examples, these weights are set as follows:

- $w = 1$ for the relevant classes "traffic signs" and "traffic lights".
- $w = 0.85$ for the classes "people" and "rider".
- $w = 0.20$ for the non-relevant classes "sky" and "vegetation".
- $w = 0.50$ for all the other classes.

After defining the loss function, the subnetwork G_s and the associate discriminator D_{disc}^s , can be trained. During training, the masking fraction m_s is randomly varied, selected from a set of values ranging from 5% to 100% with an expected value of 35%. This approach allows the model to learn to compress the SSM at various levels of compression and increase the robustness of the model with respect to different conditions of the channel. If the task will require it, it is in fact possible to dynamically adapt the masking fraction without having to train another model from scratch, like other approaches like [12], [13] and [21] do. The subnetwork G_s , and the associated discriminator D_{disc}^s , are trained using the Adam optimizer [35] with a learning rate of 10^{-4} and a batch size of 8. The training is conducted for 200 epochs with early stopping to prevent overfitting.

C. Training G_x

The training of the subnetwork G_x follows a similar approach. As said before, at this stage G_x is trained using the original image \mathbf{x} and the original SSM \mathbf{s} ,

as illustrated in Fig. 5. Again, an adversarial approach typical of VQ-GANs is employed for training, with the loss function defined as:

$$\begin{aligned} \mathcal{L}_{\text{SQ-GAN}}^{\mathbf{x}} &= \mathcal{L}_{Wl_2} + \mathcal{L}_{\text{perc}} + \\ &\quad + \lambda_{\text{GAN}} [\log D_{\text{disc}}^{\mathbf{x}}(\mathbf{x}|\mathbf{s}) + \log (1 - D_{\text{disc}}^{\mathbf{x}}(G_{\mathbf{x}}(\mathbf{x})|\mathbf{s}))] \\ &\quad + \lambda_{\text{vq}} \|\text{sg}[\mathbf{z}^{\mathbf{x}}] - \mathbf{z}_q^{\mathbf{x}}\|_2^2 + \lambda_{\text{commit}} \|\mathbf{z}^{\mathbf{x}} - \text{sg}[\mathbf{z}_q^{\mathbf{x}}]\|_2^2 \\ &:= \mathcal{L}_{Wl_2} + \mathcal{L}_{\text{perc}} + \lambda_{\text{GAN}} \mathcal{L}_{\text{GAN}} + \lambda_{\text{vq}} \mathcal{L}_{\text{vq}} + \lambda_{\text{commit}} \mathcal{L}_{\text{commit}} \end{aligned} \quad (4)$$

where the last two terms and the λ 's are defined as in (3), while the first three terms are defined as follows. The weighted ℓ_2 loss \mathcal{L}_{Wl_2} , defined as:

$$\mathcal{L}_{Wl_2}(\mathbf{x}, \hat{\mathbf{x}}) = \frac{1}{HW} \sum_{(h,w)} w_{\mathbf{s}(h,w)} \|\mathbf{x}_{(h,w)} - \hat{\mathbf{x}}_{(h,w)}\|_2^2, \quad (5)$$

is designed to adjust the importance of different semantic classes in the image. In (5), $\mathbf{x}_{(h,w)}$ and $\hat{\mathbf{x}}_{(h,w)}$ are the pixel values at location (h, w) of the tensors \mathbf{x} and $\hat{\mathbf{x}}$, respectively, and $w_{\mathbf{s}(h,w)}$ is the weight associated with the semantic class at that pixel, as given by the SSM \mathbf{s} . Specifically, while training the model used in our numerical examples, we used the following weights:

- $w = 1$ for the relevant classes "traffic signs" and "traffic lights".
- $w = 0.55$ for the classes "people" and "rider".
- $w = 0$ for the non-relevant classes "sky" and "vegetation".
- $w = 0.15$ for all other classes.

Of particular interest is the zero weight assigned to the classes "sky" and "vegetation". This allows the network to neglect the pixel-by-pixel reconstruction of these classes. In fact, the real colors of the sky and trees for the task at hand are semantically irrelevant.

The perceptual loss $\mathcal{L}_{\text{perc}}$ is instead the part that ensures that the reconstructed image maintains visual similarity to the original, preventing unrealistic alterations such as an unnatural sky color. To quantify this loss, we used Learned Perceptual Image Patch Similarity (LPIPS) [36], which evaluates the difference between two images in a latent space representation. The underlying idea is that if two images convey similar semantic content, for example, if they both contain relevant objects such as pedestrians, cars, or traffic lights, each with the correct shape and positioned appropriately relative to one another, the semantic distortion should be low, regardless of any differences at the pixel level. LPIPS, instead of computing pixel-wise differences between \mathbf{x} and $\hat{\mathbf{x}}$, compares the latent features extracted from the images by employing a deep neural network (DNN) pre-trained for object recognition. The DNN is somehow substituting a

human to quantify the perceptual difference between two images. Formally, LPIPS is defined as:

$$\mathcal{L}_{\text{perc}} = \sum_{l \in L} \frac{1}{H_l W_l} \sum_{(h_j, w_j)} \|\mathbf{w}_l \odot (\phi_l(\mathbf{x}) - \phi_l(\hat{\mathbf{x}}))\|_2^2$$

where $\phi_l(\cdot)$ denotes the activation from the l -th layer of a pre-trained network ϕ , L is the set of layers used for feature extraction, H_l and W_l are the height and width of the feature map at layer l , and \mathbf{w}_l are learned weights that adjust the contribution of each layer. The operator \odot denotes element-wise multiplication between the weight \mathbf{w}_l and all the elements of the difference $(\phi_l(\mathbf{x}) - \phi_l(\hat{\mathbf{x}}))$ in any location coordinate (h_j, w_j) . By comparing the feature representations at multiple layers, LPIPS captures perceptual differences at different scales and abstraction levels. Lower LPIPS values indicate better reconstruction quality.

Another important novel aspect of the proposed approach is the adversarial loss \mathcal{L}_{GAN} involving a new semantic-aware discriminator network. The discriminator $D_{\text{disc}}^{\mathbf{x}}$ plays a crucial role in adversarial training by determining whether an image reconstructed by $G_{\mathbf{x}}$ is real or fake. However, a potential drawback is that the discriminator might focus on non-relevant parts of the image to produce its classification score. For instance, it might prioritize vegetation details, and classify images as real only if the leaves on the trees have a certain level of detail. This will force the generator $G_{\mathbf{x}}$ to reconstruct images with better vegetation details to fool the discriminator. Unfortunately, this is not optimal for the structure of the SQ-GAN. Giving more importance to the vegetation will decrease the importance of other classes, thus causing the SAMM module to select the wrong latent vectors as relevant.

In recent years, several works have proposed ways to modify the discriminator by introducing various conditioning. For example, [37] conditioned the discriminator on the SSM to improve Semantic Segmentation (SSeg) retention, while [38] enforced the discriminator to focus on high frequency components. However, these methods do not adequately address the issue at hand. To achieve the desired performance, it is essential to adjust the discriminator to minimize its focus on non-relevant regions. To this end, we make the following observations about the discriminator's behavior:

- For a (generic) trained discriminator D_{disc} and two images \mathbf{x} and \mathbf{y} , $D_{\text{disc}}(\mathbf{x})$ is likely similar to $D_{\text{disc}}(\mathbf{y})$ if both images originate from the same data distribution, i.e., $p_{\mathbf{x}} = p_{\mathbf{y}}$. However, $D_{\text{disc}}(\mathbf{x}) = D_{\text{disc}}(\mathbf{y})$ is not guaranteed unless the images are identical or indistinguishable by the discriminator.
- If $p_{\mathbf{y}}$ differs from $p_{\mathbf{x}}$, $D_{\text{disc}}(\mathbf{y})$ will likely differ from $D_{\text{disc}}(\mathbf{x})$. The output difference is primarily

influenced by the aspects of p_y that deviate from p_x .

- The greater the difference between p_x and p_y , the higher the uncertainty in predicting $D_{disc}(y)$ based on $D_{disc}(x)$.

Based on these insights, we propose to reduce the discriminator's focus on non-relevant semantic classes. Our approach consists of artificially modifying the reconstructed image \hat{x} before it is evaluated by the discriminator and in (4) has been represented as conditioning the input of the discriminator as $D_{disc}^x(\cdot|s)$. This modification aims to minimize the differences in non-relevant regions between x and \hat{x} , bringing the data distribution of these regions of \hat{x} closer to the real distribution of x . For example, if the generator reconstructs a tree with dark green leaves when in reality they are light green, the color in \hat{x} will be artificially shifted toward light green.

This artificial editing is performed by considering the residual between the real and reconstructed images, defined as $r = x - \hat{x}$. By using the SSM to mask the pixel-wise difference between the two images, and adding back a fraction of the residual to \hat{x} it is possible to obtain the new image $\hat{x}_{rel} = \hat{x} + w_{rel} \odot r$. In this context w_{rel} represents the re-scaling relevance tensor that is obtained as a function of the SSM s and has the same shape as for the images, namely shape $3 \times H \times W$. The element (i, h, w) of the tensor w_{rel} is obtained from s by assigning the following values based on the class of the pixel (h, w) . In particular, in the training for our numerical examples, we used:

- $w = 0.90$ for the class "sky".
- $w = 0.80$ for the class "vegetation".
- $w = 0.40$ for the class "street".
- $w = 0$ for the other classes.

For example, this means that 80% of the difference between the shades of green leaves is removed before presenting the image to the discriminator. The modified vegetation in \hat{x}_{rel} will appear much closer to the real light green in x , thus reducing the discriminator's focus on this non-relevant region. It is important to acknowledge that this approach negatively impacts the generator's ability to accurately reproduce these specific non-relevant classes. Nevertheless, the perceptual loss still considers the entire image, guiding the generator to reconstruct the "sky," "vegetation," and "streets" to maintain overall realism.

The sub-network G_x is trained for different masking fractions m_x , similarly to G_s , to increase the robustness of the model with respect to different conditions of the channel. These values are selected from a finite set ranging from 5% to 100% with an expected value of 35%. The structure of D_{disc}^x is the same as D_{disc}^s and the training is performed using the Adam optimizer with

a learning rate of 10^{-4} with batch size of 8. The model is trained for 200 epochs with early stopping.

D. Fine-tuning G

The final step involves fine-tuning the entire network G by freezing the parameters of G_s and updating only those of G_x . This fine-tuning addresses the scenario where the original SSM s is unavailable at the receiver, that is, when the SQ-GAN is used for Semantic Communication (SC). Notice that the fine-tuning step is *essential* since the quality of \hat{s} is influenced by the masking fraction m_s , and this dependency is missed in the separate training steps described above. The loss function and the semantic-aware discriminator D_{disc}^x remain identical to those used in the training of G_x . Fine-tuning is conducted over 100 epochs with early stopping to prevent overfitting. During each iteration, both masking fractions m_x and m_s are randomly selected from the same distribution. The Adam optimizer is employed with a learning rate of 10^{-4} and a batch size of 8.

V. RESULTS

This section focuses on the performance of the proposed SQ-GAN evaluated using 500 images (and corresponding SSMs) from the validation set of the Cityscapes dataset [30]. In Section V-A, we illustrate the function and role of the SAMM in selecting features of x and s that are semantically relevant. Furthermore, we also show the effect of masking fractions on the final reconstruction. In Section V-B the performance of the proposed SQ-GAN is compared with SOTA compression algorithms like BPG, JPEG2000 and deep-learning based alternatives such as HiFiC [12] and FCC [13]. For the selection of the deep learning-based comparison methods, we considered only those providing the open source code and the model weights. Furthermore, we have not considered methods designed for JSCC, since we consider only source coding.

We also computed the SSM \tilde{s} of the reconstructed image \hat{x} and compared it with the SSM s of the original image, to quantitatively assess the capability of the coding method to preserve some semantics aspects of the image to be transmitted, such as identification of objects like "pedestrians", "traffic signs", etc., the estimation of their shape and of their relative positioning.

A. SAMM function

SQ-GAN adopts various techniques to force the model to correctly reconstruct the relevant regions of the image. The weighted loss function based on the semantic classes, the semantic-aware discriminator D_{disc}^x , and the data augmentation step described in IV-A, have been designed with this idea in mind. Their scope is to guide

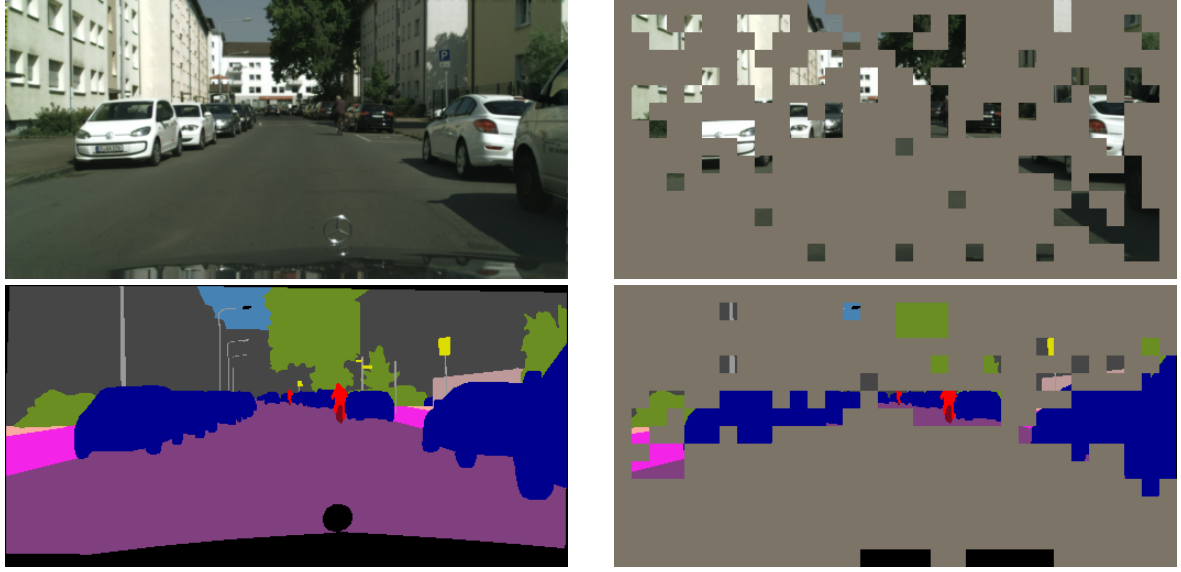


Figure 7: Visual representation of the latent tensor selection of the SAMM projected in the image and SSM domain. In both cases the masking has been fixed to $m_x = m_s = 0.20$ and the regions considered semantically relevant are shown on the right.

SAMM to identify and select the relevant latent vectors z_k^x and z_k^s . Since the selection is performed on the latent tensor, to understand the effect of SAMM, we project back from the latent tensor to the image (pixel) domain [21]. Fig. 7 shows such a projection for a specific example.² The left column displays the original x and s , whereas the right column indicates the regions associated with the latent vectors deemed most relevant by SAMM. In this example, the masking fractions are chosen as $m_x = m_s = 0.20$.

It is immediately evident that G_x and G_s consider different regions as relevant. The SAMM in G_s focuses on regions with the most change in semantic classes. Streets, buildings, and the sky require very few associated latent vectors for their representation. In contrast, the regions of the SSM containing semantically relevant classes are strongly prioritized.

Similarly, the SAMM in G_x shows a strong preference for relevant classes like cars and people. However, it also focuses on areas previously ignored, such as the street and the buildings. Indeed, thanks to the conditioning on the SSM, the sub-network G_x is aware of the location and shape of each relevant object, allowing it to focus on other aspects such as colors and textures. As a result, elements like the streets and the sky still require some latent vectors to accurately reconstruct their colors.

²The projection shown in figure 7 was implemented by leveraging the convolutional structure of the two encoders that allows to trace back the spatial correlation between the latent tensor and the original frame.

However, most of the latent vectors are selected from the truly relevant regions.

In both cases, SAMM tends to prefer regions that contain more semantically relevant objects. This is a direct effect of the various techniques adopted to train the model as described in Section IV.

Next, we examine the effect of different masking fractions on the quality of the reconstructed image and SSM. In fact increasing m_x and m_s is expected to increase the overall quality of \hat{x} and \hat{s} respectively, while decreasing is expected to do the opposite. Fig. 8 shows visually how masking fractions influence the reconstructed outputs.

The column on the left shows the original x and s . The other columns show on top the reconstructed \hat{x} and the generated SSM obtained from \hat{x} via the INTERN-2.5 SSMModel [22]. The bottom row shows the reconstructed \hat{s} . These examples are obtained by fixing the compression level to a total amount of 0.05 BPP and by letting the masking fractions m_x and m_s to vary, while keeping their sum constant. In this example, $m_x + m_s = 1.1$.

The quality of \hat{x} is significantly affected by the fidelity of \hat{s} , which depends heavily on m_s , more than m_x . A reduction in object detail within \hat{s} directly limits the ability of \hat{x} to retain such details. This is evident by comparing the bottom row \hat{s} with the generated SSM in the upper row: any detail absent in \hat{s} is also absent in the SSM.

Conversely, the influence of m_x on the overall quality exhibits the expected behavior: increasing m_x enhances

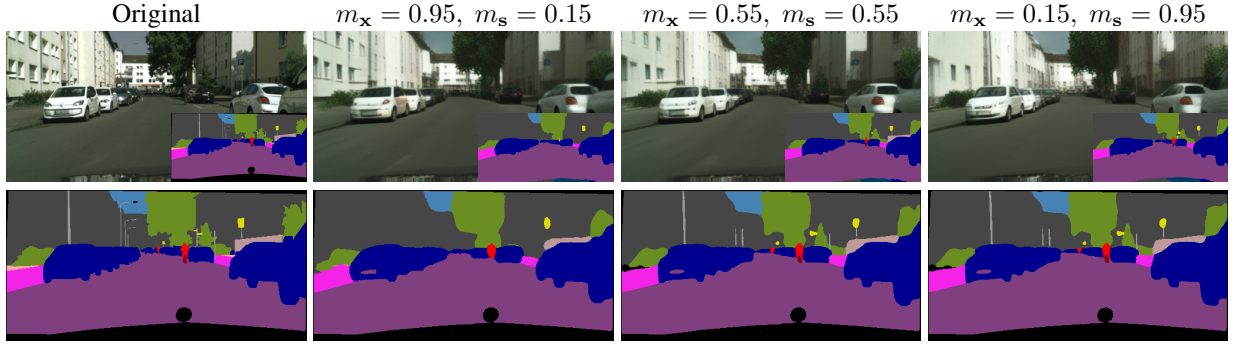


Figure 8: Visual comparison between the same image and SSM at different masking reactions m_x and m_s . The original image and SSM are shown on the left. The upper row shows the reconstructed \hat{x} and the generated SSM using the SOTA SSModel INTERN-2.5 [22]. The bottom row shows the reconstructed SSM \hat{s} . All pairs (\hat{x}, \hat{s}) are obtained at 0.05BPP.

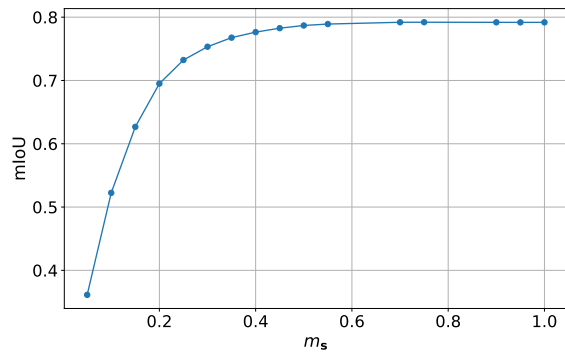


Figure 9: SSM retention evaluated as the mIoU between the true s and the reconstructed \hat{s} as a function of the masking fraction m_s . As the masking fraction m_s increases the network G_s is able to better reconstruct the SSM. However, the increase of performance reaches a plateau from $m_s \geq 0.2$ ($BPP_s = 0.011$ BPP).

image fidelity, particularly for non-relevant details. Relevant features are prioritized and reconstructed effectively even at low values of m_x , whereas finer details, such as building windows, are better preserved when $m_x = 0.95$. This demonstrates the model's capability to prioritize semantically relevant features before refining non-relevant aspects of the image.

To assess the quality of the reconstructed SSM, we use the mean Intersection over Union (mIoU) parameter, defined as:

$$\text{mIoU} = \frac{1}{n_c} \sum_{i=1}^{n_c} \frac{|s_i \cap s'_i|}{|s_i \cup s'_i|},$$

where n_c represents the number of semantic classes, and s_i and s'_i are pixel sets of class i in s and the predicted s' , respectively. This parameter measures how well two

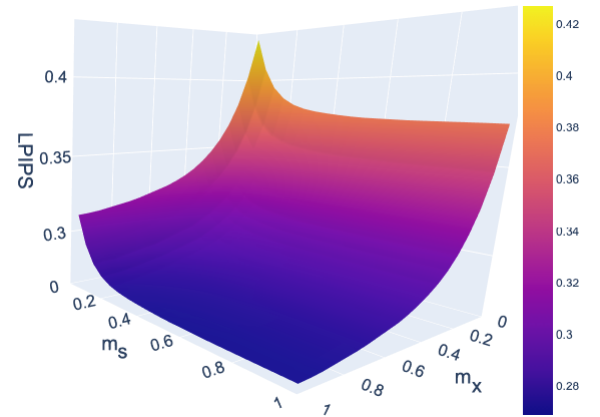


Figure 10: LPIPS evaluated between x and \hat{x} as the masking fractions m_s and m_x vary. By properly selecting the masking fractions it is possible to reduce the redundancy, while preserving a task-specific feature, represented by the LPIPS value

segmentation maps overlap with each other. A value close to 1 indicates a high semantic content retention in \hat{x} .

The impact of m_s on the mIoU is illustrated in Fig. 9. It is useful to notice that, for $m_s \geq 0.55$, the value of mIoU remains almost constant. This means that, above that value, additional latent vectors do not add relevant semantic features. For very low values of m_s the performance is poor, but, as soon as $m_s \geq 0.20$, the model is able to reconstruct \hat{s} with an acceptable level of semantic retention. To give a term of comparison, the value of $m_s = 0.20$ corresponds to a compression of $BPP_s = 0.011$ BPP. This means that at this low value of BPP the model is already able to preserve valuable details in the SSM. Increasing m_s beyond the value of 0.55 (equivalent to $BPP_s = 0.025$ BPP) does not provide further improvement. We interpret this saturation

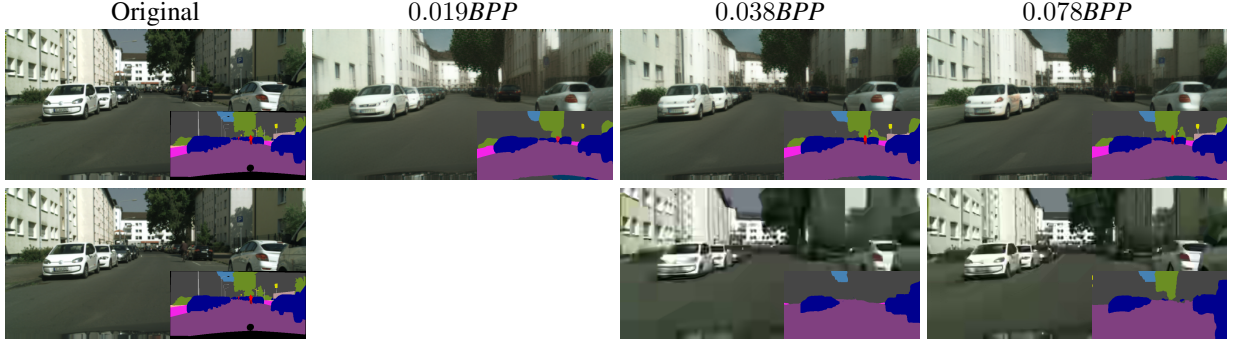


Figure 11: Visual comparison at different compression rates between the proposed SQ-GAN (TOP) and the classical BPG (BOTTOM). The SSMs shown are generated from $\hat{\mathbf{x}}$ via the SOTA SSModel INTERN-2.5 [22]. The proposed model is able to reconstruct images with higher semantic retention and lower values of BPP compared with BPG. The BPG algorithm is not able to compress images at lower values than 0.038 BPP, thus the comparison is limited to 0.038 and 0.078 BPP.

as follows: beyond this value, all semantically relevant latent vectors have been selected and quantized. Adding other vectors will only increase the amount of redundant information, without improving the reconstructed SSM. This behavior is quite different from what was observed and discussed previously about m_x , where even for values close to 1, the improvements were still visible on the final output.

It is also interesting to see how both m_x and m_s affect $\hat{\mathbf{x}}$. For this purpose, in Fig. 10 we report the value of LPIPS to measure the distance between \mathbf{x} and $\hat{\mathbf{x}}$ and show the importance of semantic masking. As expected, the performance along the m_s axis has a strong influence on the output only for values of $m_s \leq 0.55$. Instead, the influence of m_x is observed along the whole range from 0 to 1. This is consistent with the visual results shown in Fig. 8 and show how, by properly selecting the masking coefficients m_x and m_s , we can strongly reduce the redundancy, while preserving a task-specific feature, represented by the LPIPS value.

B. Visual Results and Comparisons with SOTA image compression

In this section, the results of the proposed SQ-GAN are compared with the SOTA conventional algorithms BPG and JPEG2000, and with deep-learning-based compression algorithms HiFiC [12] and FCC [13]. A visual comparison between BPG and SQ-GAN is shown in Fig. 11.

The top row represents the reconstructed image $\hat{\mathbf{x}}$ obtained with the proposed SQ-GAN and the associated SSM generated via the INTERN-2.5 SSModel. The bottom row shows the reconstructed image obtained by using the BPG algorithm and the associated generated SSM. We notice that SQ-GAN can reach lower values

of BPP. In particular, in this case BPG cannot compress images at BPP lower than 0.038. Furthermore, while BPG uses precious resources to reconstruct semantically irrelevant details such as the windows of the buildings, SQ-GAN focuses on the relevant parts. This is further evidenced by the amount of semantic retention of the generated SSM. For example, the cyclist on the bike is still visible and can be correctly identified by SSModel, at all levels of BPP in Fig. 11. In contrast, the cyclist completely disappears in the generated SSM from the BPG reconstructed image at all levels of BPP in Fig. 11. As a comparison term, to obtain a level of semantic retention similar to the one obtained by SQ-GAN at 0.038 BPP, BPG requires a rate of 0.280 BPP.

As a further parameter used to quantify the (semantic) distortion between the original and reconstructed images, we used the Fréchet Inception Distance (FID), evaluated over a batch of images [39]. The value of FID is defined as [39]:

$$\text{FID} = \left\| \mu_{\phi}(\mathbf{X}) - \mu_{\phi}(\hat{\mathbf{X}}) \right\|_2^2 + \text{Tr} \left(\Sigma_{\phi}(\mathbf{x}) + \Sigma_{\phi}(\hat{\mathbf{X}}) - 2 \left(\Sigma_{\phi}(\mathbf{X}) \Sigma_{\phi}(\hat{\mathbf{X}}) \right)^{1/2} \right)$$

where \mathbf{X} and $\hat{\mathbf{X}}$ are the sets of real and reconstructed images, respectively; $\mu_{\phi}(\mathbf{X})$ and $\Sigma_{\phi}(\mathbf{X})$ are the mean and covariance of the features extracted from the real images \mathbf{X} using a pre-trained Inception-v3 model ϕ [40]; $\mu_{\phi}(\hat{\mathbf{X}})$ and $\Sigma_{\phi}(\hat{\mathbf{X}})$ are the corresponding statistics from the reconstructed images $\hat{\mathbf{X}}$. Rather than directly comparing images pixel by pixel, the FID compares the distributions of the latent representations of the original and reconstructed images obtained using a convolutional neural network (Inception v3) trained for image

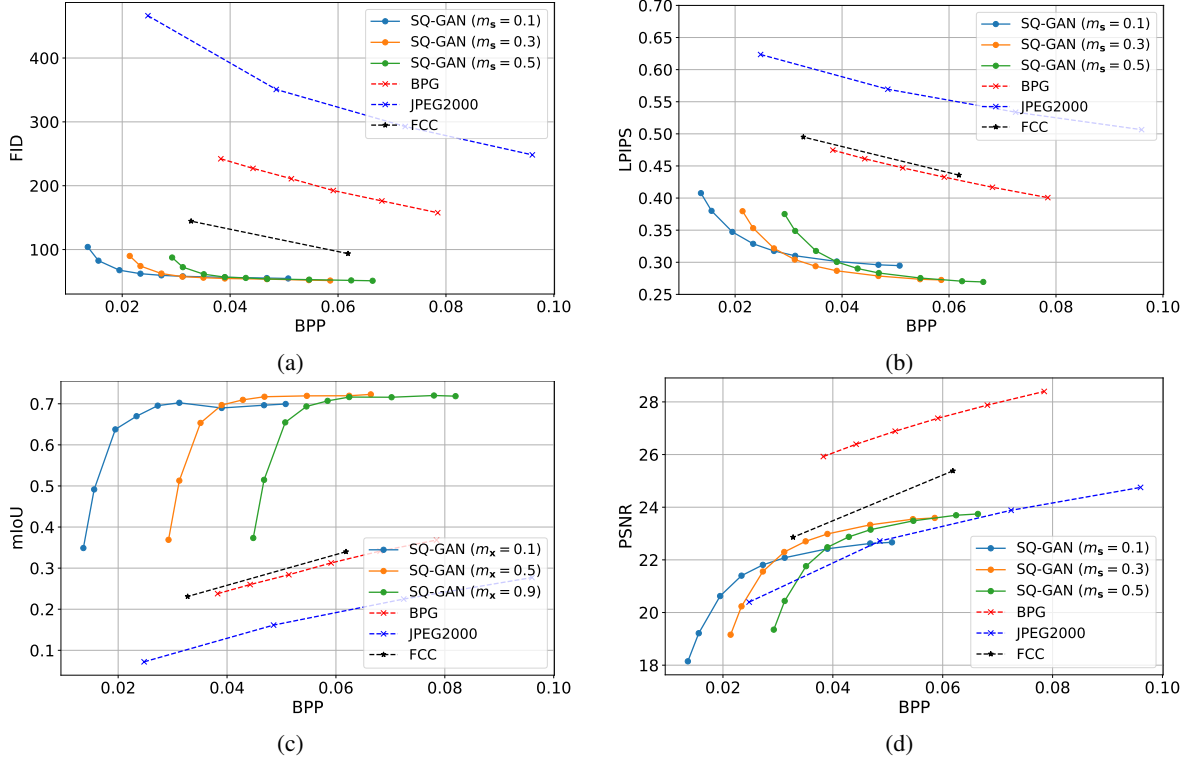


Figure 12: Performance comparison between BPG, JPEG2000 and SQ-GAN in terms of semantic metrics and the classic pixel-by-pixel PSNR.

recognition. From its definition, FID is a parameter that is robust against translation, rotation, or change of scale of relevant objects. A low value of FID indicates that a DNN operating over the two batches of original and reconstructed images extract representations that are statistically equivalent.

To assess the performance of SQ-GAN, we compare it with established SOTA image encoders, including JPEG2000, BPG, FCC, and HiFiC, using four metrics: FID, LPIPS, Peak Signal-to-Noise Ratio (PSNR), and mIoU. The first three metrics are computed between the original image \mathbf{x} and its reconstruction $\hat{\mathbf{x}}$, while the mean Intersection over Union (mIoU) is evaluated between the original semantic segmentation map \mathbf{s} and the SSM $\tilde{\mathbf{s}}$, generated from $\hat{\mathbf{x}}$ using the SOTA INTERN-2.5 SSModel. The quantitative results are shown in Fig. 12, which plots each metric as a function of BPP, as defined in (2).

We begin by examining how SQ-GAN compares to approaches that are able to compress the image at comparable values of BPP, namely JPEG2000, BPG, and FCC. As evident from Fig. 12, SQ-GAN significantly outperforms these methods on semantic-aware metrics such as FID, LPIPS, and mIoU, which better reflect perceptual and task-related image quality. SQ-GAN is outperformed by BPG and FCC on PSNR, a pixel-level

distortion measure, which favors pixel-by-pixel recovery rather than semantic relevance.

It is important to note that SQ-GAN is capable of operating effectively even at very low bitrates. For instance, even at approximately 0.01 BPP, it preserves meaningful semantic structures, as demonstrated by favorable FID, LPIPS, and mIoU scores. It is also interesting to observe what happens at BPP = 0.038. BPG reconstructs images with a PSNR of 26, outperforming SQ-GAN in terms of pixel fidelity. However, as shown in Fig. 11, BPG fails to preserve important semantic content. In fact, only the first two cars in the scene are detected while the distant pedestrian and the traffic signs are lost. In contrast, SQ-GAN maintains better object-level consistency.

The comparison with the FCC model further highlights the efficiency of SQ-GAN in semantic preservation. For example, FCC achieves an FID=93 at a BPP of 0.061, whereas SQ-GAN attains the same FID at a BPP of 0.017, indicating a bitrate reduction factor of approximately 3.6 times to achieve comparable reconstructed image quality. Similar trends are observed in LPIPS and mIoU, reinforcing the semantic coding advantage of our model.

Finally, we considered the HiFiC model, a High-Fidelity Generative Image Compression method often adopted as a benchmark. We chose not to include HiFiC

in Fig. 12, as its operational BPP range begins at 0.142, which is substantially higher than the range analyzed for the other models in the figure (from 0.015 to 0.08 BPP). Working at BPP = 0.142, HiFiC yields superior performance in terms of PSNR= 28.34, FID= 35.47, and LPIPS= 0.223, as expected, because of the much higher BPP. Nevertheless, it is impressive to notice that, in terms of mIoU, HiFiC reaches only a value of 0.565, i.e., the same value attained by SQ-GAN at BPP = 0.018, which corresponds to a rate reduction factor of about 7.8 times. This underlines the remarkable semantic compression capability of SQ-GAN, even when compared with high-performing learned codecs at significantly higher bitrates.

VI. CONCLUSIONS

This work presents SQ-GAN, a new approach for simultaneous encoding of images and their semantic maps, aimed at preserving the image semantic content, even at very low coding rates. The comparison of SQ-GAN with SOTA encoders has been carried out using a set of perceptual performance indicators, like FID, LPIPS, and mIoU, that somehow measure the semantic distortion between the original image (or semantic map) and the reconstructed image (or semantic map). Using these performance indicators, extensive evaluations on the Cityscapes dataset show that SQ-GAN significantly outperforms JPEG2000, BPG, FCC and HiFiC, in terms of rate-(semantic) distortion trade-off. At the same time, SQ-GAN is clearly outperformed by BPG and FCC in terms of conventional pixel-level indicators, such as the PSNR. In summary, SQ-GAN significantly outperforms state-of-the-art image encoders in semantic-aware image compression tasks, whose primary goal is not perfect pixel-level reconstruction, but rather the preservation of semantic contents that are more important for high-level vision tasks.

We tested our method on the autonomous driving use case, but our approach can be applied to many other scenarios, like medical imaging, remote sensing, space exploration, etc., whenever there is a need to strongly compress the images, while retaining as much as possible their semantic content. Nevertheless, also the autonomous driving use case offers useful motivations for using our coding scheme, like reducing the traffic load necessary to send images to a remote server for training autonomous driving models; or strongly compressing images for liability assessment in case of accidents, while preserving critical semantic details (e.g., traffic lights, road signs, pedestrians). Further investigations are in progress to simplify the coding strategy, optimize the shapes of the image and semantic map tensors and generalize the approach to video coding.

ACKNOWLEDGMENT

This work was supported by the Gottfried Wilhelm Leibniz-Preis 2021 of the German Science Foundation (DFG), Joint Project 6G-RIC (Project IDs 16KISK030), the Italian National Recovery and Resilience Plan (NRRP) of NextGenerationEU, partnership on “Telecommunications of the Future” (PE00000001 - program RESTART), Huawei Technology France SASU, under agreement N.TC20220919044, and the SNS-JU-2022 project ADROIT6G under agreement n. 101095363.

REFERENCES

- [1] H. Yang, A. Alphones, Z. Xiong, D. Niyato, J. Zhao, and K. Wu, “Artificial-intelligence-enabled intelligent 6g networks,” *IEEE network*, vol. 34, no. 6, pp. 272–280, 2020.
- [2] E. Calvanese Strinati and S. Barbarossa, “6g networks: Beyond Shannon towards semantic and goal-oriented communications,” *Computer Networks*, vol. 190, pp. 1–17, 2021.
- [3] H. Xie, Z. Qin, G. Y. Li, and B.-H. Juang, “Deep learning enabled semantic communication systems,” *IEEE Transactions on Signal Processing*, vol. 69, pp. 2663–2675, 2021.
- [4] D. Gündüz, Z. Qin, I. E. Aguerri, H. S. Dhillon, Z. Yang, A. Yener, K. K. Wong, and C.-B. Chae, “Beyond transmitting bits: Context, semantics, and task-oriented communications,” *IEEE Journal on Selected Areas in Communications*, vol. 41, no. 1, pp. 5–41, 2022.
- [5] H. Xie, Z. Qin, X. Tao, and K. B. Letaief, “Task-oriented multi-user semantic communications,” *IEEE Journal on Selected Areas in Communications*, vol. 40, no. 9, pp. 2584–2597, 2022.
- [6] W. Yang, H. Du, Z. Q. Liew, W. Y. B. Lim, Z. Xiong, D. Niyato, X. Chi, X. Shen, and C. Miao, “Semantic communications for future internet: Fundamentals, applications, and challenges,” *IEEE Communications Surveys & Tutorials*, vol. 25, no. 1, pp. 213–250, 2022.
- [7] S. Barbarossa, D. Communiello, E. Grassucci, F. Pezone, S. Sardellitti, and P. Di Lorenzo, “Semantic communications based on adaptive generative models and information bottleneck,” *IEEE Communications Magazine*, vol. 61, no. 11, pp. 36–41, 2023.
- [8] Z. Tao, W. Xu, Y. Huang, X. Wang, and X. You, “Wireless network digital twin for 6g: Generative ai as a key enabler,” *IEEE Wireless Communications*, vol. 31, no. 4, pp. 24–31, 2024.
- [9] N. Van Huynh, J. Wang, H. Du, D. T. Hoang, D. Niyato, D. N. Nguyen, D. I. Kim, and K. B. Letaief, “Generative ai for physical layer communications: A survey,” *IEEE Transactions on Cognitive Communications and Networking*, 2024.
- [10] S. Tang, Q. Yang, D. Gündüz, and Z. Zhang, “Evolving semantic communication with generative modelling,” in *2024 IEEE 35th International Symposium on Personal, Indoor and Mobile Radio Communications (PIMRC)*. IEEE, 2024, pp. 1–6.
- [11] H. Xie, Z. Qin, G. Y. Li, and B.-H. Juang, “Deep learning enabled semantic communication systems,” *IEEE Transactions on Signal Processing*, vol. 69, pp. 2663–2675, 2021.
- [12] F. Mentzer, G. D. Toderici, M. Tschannen, and E. Agustsson, “High-fidelity generative image compression,” *Advances in Neural Information Processing Systems*, vol. 33, 2020.
- [13] S. Iwai, T. Miyazaki, Y. Sugaya, and S. Omachi, “Fidelity-controllable extreme image compression with generative adversarial networks,” 01 2021, pp. 8235–8242.
- [14] J. Xu, T.-Y. Tung, B. Ai, W. Chen, Y. Sun, and D. Gündüz, “Deep joint source-channel coding for semantic communications,” *IEEE communications Magazine*, vol. 61, no. 11, pp. 42–48, 2023.
- [15] Z. Weng and Z. Qin, “Semantic communication systems for speech transmission,” *IEEE Journal on Selected Areas in Communications*, vol. 39, no. 8, pp. 2434–2444, 2021.

- [16] I. Goodfellow, J. Pouget-Abadie, M. Mirza, B. Xu, D. Warde-Farley, S. Ozair, A. Courville, and Y. Bengio, "Generative adversarial nets," in *Advances in neural information processing systems*, 2014, pp. 2672–2680.
- [17] S. Liu, Z. Peng, Q. Yu, and L. Duan, "A novel image semantic communication method via dynamic decision generation network and generative adversarial network," *Scientific Reports*, vol. 14, 08 2024.
- [18] F. Pezone, O. Musa, G. Caire, and S. Barbarossa, "Semantic-preserving image coding based on conditional diffusion models," in *ICASSP 2024-2024 IEEE International Conference on Acoustics, Speech and Signal Processing (ICASSP)*. IEEE, 2024, pp. 13 501–13 505.
- [19] A. van den Oord, O. Vinyals, and K. Kavukcuoglu, "Neural discrete representation learning," in *Proceedings of the 31st International Conference on Neural Information Processing Systems*, ser. NIPS'17. Red Hook, NY, USA: Curran Associates Inc., 2017, p. 6309–6318.
- [20] P. Esser, R. Rombach, and B. Ommer, "Taming transformers for high-resolution image synthesis," in *CVPR*. Computer Vision Foundation / IEEE, 2021, pp. 12 873–12 883. [Online]. Available: <http://dblp.uni-trier.de/db/conf/cvpr/cvpr2021.html#EsserRO21>
- [21] M. Huang, Z. Mao, Q. Wang, and Y. Zhang, "Not all image regions matter: Masked vector quantization for autoregressive image generation," in *Proceedings of the IEEE/CVF Conference on Computer Vision and Pattern Recognition (CVPR)*, June 2023, pp. 2002–2011.
- [22] W. Wang, J. Dai, Z. Chen, Z. Huang, Z. Li, X. Zhu, X. Hu, T. Lu, L. Lu, H. Li *et al.*, "InternImage: Exploring large-scale vision foundation models with deformable convolutions," *arXiv preprint arXiv:2211.05778*, 2022.
- [23] M. A. Elhassan, C. Zhou, A. Khan, A. Benabid, A. B. Adam, A. Mehmood, and N. Wambugu, "Real-time semantic segmentation for autonomous driving: A review of cnns, transformers, and beyond," *Journal of King Saud University-Computer and Information Sciences*, p. 102226, 2024.
- [24] Tesla, Inc. (2025) AI & Robotics. Tesla. [Online]. Available: <https://www.tesla.com/AI>
- [25] K. He, X. Zhang, S. Ren, and J. Sun, "Deep residual learning for image recognition," in *2016 IEEE Conference on Computer Vision and Pattern Recognition (CVPR)*, 2016, pp. 770–778.
- [26] A. Dosovitskiy, L. Beyer, A. Kolesnikov, D. Weissenborn, X. Zhai, T. Unterthiner, M. Dehghani, M. Minderer, G. Heigold, S. Gelly, J. Uszkoreit, and N. Houlsby, "An image is worth 16x16 words: Transformers for image recognition at scale," in *International Conference on Learning Representations*, 2021. [Online]. Available: <https://openreview.net/forum?id=YicbFdNTTy>
- [27] T. Park, M.-Y. Liu, T.-C. Wang, and J.-Y. Zhu, "Semantic image synthesis with spatially-adaptive normalization," in *2019 IEEE/CVF Conference on Computer Vision and Pattern Recognition (CVPR)*, 2019, pp. 2332–2341.
- [28] R. Krichevsky and V. Trofimov, "The performance of universal encoding," *IEEE Transactions on Information Theory*, vol. 27, no. 2, pp. 199–207, 1981.
- [29] O. Ronneberger, P. Fischer, and T. Brox, *U-Net: Convolutional Networks for Biomedical Image Segmentation*. Cham: Springer International Publishing, 2015, pp. 234–241. [Online]. Available: https://doi.org/10.1007/978-3-319-24574-4_28
- [30] M. Cordts, M. Omran, S. Ramos, T. Rehfeld, M. Enzweiler, R. Benenson, U. Franke, S. Roth, and B. Schiele, "The cityscapes dataset for semantic urban scene understanding," in *Proc. of the IEEE Conference on Computer Vision and Pattern Recognition (CVPR)*, 2016.
- [31] A. Konushin, B. Faizov, and V. Shakhuro, "Road images augmentation with synthetic traffic signs using neural networks," *Computer Optics*, vol. 5, pp. 736–748, 09 2021.
- [32] L. Jöckel, M. Kläs, and S. Martínez-Fernández, "Safe traffic sign recognition through data augmentation for autonomous vehicles software," in *2019 IEEE 19th International Conference on Software Quality, Reliability and Security Companion (QRS-C)*, 2019, pp. 540–541.
- [33] P. Isola, J.-Y. Zhu, T. Zhou, and A. A. Efros, "Image-to-image translation with conditional adversarial networks," in *2017 IEEE Conference on Computer Vision and Pattern Recognition (CVPR)*, 2017, pp. 5967–5976.
- [34] B. Xu, N. Wang, T. Chen, and M. Li, "Empirical evaluation of rectified activations in convolutional network," *CoRR*, vol. abs/1505.00853, 2015. [Online]. Available: <http://arxiv.org/abs/1505.00853>
- [35] D. Kingma and J. Ba, "Adam: A method for stochastic optimization," in *International Conference on Learning Representations (ICLR)*, San Diego, CA, USA, 2015.
- [36] R. Zhang, P. Isola, A. A. Efros, E. Shechtman, and O. Wang, "The unreasonable effectiveness of deep features as a perceptual metric," in *CVPR*, 2018.
- [37] A. Oluwasanmi, M. U. Aftab, A. Shokanbi, J. Jackson, B. Kumeda, and Z. Qin, "Attentively conditioned generative adversarial network for semantic segmentation," *IEEE Access*, vol. 8, pp. 31 733–31 741, 2020.
- [38] Y. Chen, G. Li, C. Jin, S. Liu, and T. Li, "Ssd-gan: Measuring the realness in the spatial and spectral domains," in *AAAI*, 2021.
- [39] M. Heusel, H. Ramsauer, T. Unterthiner, B. Nessler, and S. Hochreiter, "Gans trained by a two time-scale update rule converge to a local nash equilibrium," in *Advances in Neural Information Processing Systems*, vol. 30. Curran Associates, Inc., 2017.
- [40] C. Szegedy, V. Vanhoucke, S. Ioffe, J. Shlens, and Z. Wojna, "Rethinking the inception architecture for computer vision," *2016 IEEE Conference on Computer Vision and Pattern Recognition (CVPR)*, pp. 2818–2826, 2015.

VII. BIOGRAPHY SECTION



Francesco Pezone received his B.Sc. in Physics from the University of Rome Tor Vergata, his M.Sc. in Data Science from Sapienza University of Rome, and dual Ph.D. degrees in Data Science from Sapienza University of Rome and Engineering from Technische Universität Berlin. He is an AI researcher specializing in generative AI, computer vision, and optimization theory, with a focus on efficient data compression and semantic communication.



Sergio Barbarossa is a Full Professor at Sapienza University of Rome and a Senior Research Fellow of Sapienza School for Advanced Studies (SSAS). He is an IEEE Fellow and a EURASIP Fellow. He received the Technical Achievements Award from the European Association for Signal Processing (EURASIP) society in 2010 and the IEEE Signal Processing Society Best Paper Awards in the years 2000, 2014, and 2020, and. He was an IEEE Distinguished Lecturer in 2013–

2014. He has been the scientific coordinator of several European projects and he is now coordinating a national project called "Network Intelligence" and a national initiative named "Make Artificial Intelligence Distributed and Networked". His main current research interests include semantic and goal-oriented communications, topological signal processing and learning, 6G networks and distributed edge machine learning.



Giuseppe Caire (S '92 – M '94 – SM '03 – F '05) was born in Torino in 1965. He received a B.Sc. in Electrical Engineering from Politecnico di Torino in 1990, an M.Sc. in Electrical Engineering from Princeton University in 1992, and a Ph.D. from Politecnico di Torino in 1994. He has been a post-doctoral research fellow with the European Space Agency (ESTEC, Noordwijk, The Netherlands) in 1994-1995, Assistant Professor in Telecommunications at the Politecnico

di Torino, Associate Professor at the University of Parma, Italy, Professor with the Department of Mobile Communications at the Eurecom Institute, Sophia-Antipolis, France, a Professor of Electrical Engineering with the Viterbi School of Engineering, University of Southern California, Los Angeles, and he is currently an Alexander von Humboldt Professor with the Faculty of Electrical Engineering and Computer Science at the Technical University of Berlin, Germany.

He received the Jack Neubauer Best System Paper Award from the IEEE Vehicular Technology Society in 2003, the IEEE Communications Society and Information Theory Society Joint Paper Award in 2004, in 2011, and in 2025, the Okawa Research Award in 2006, the Alexander von Humboldt Professorship in 2014, the Vodafone Innovation Prize in 2015, an ERC Advanced Grant in 2018, the Leonard G. Abraham Prize for best IEEE JSAC paper in 2019, the IEEE Communications Society Edwin Howard Armstrong Achievement Award in 2020, the 2021 Leibniz Prize of the German National Science Foundation (DFG), and the CTTC Technical Achievement Award of the IEEE Communications Society in 2023. Giuseppe Caire is a Fellow of IEEE since 2005. He has served in the Board of Governors of the IEEE Information Theory Society from 2004 to 2007, and as officer from 2008 to 2013. He was President of the IEEE Information Theory Society in 2011. His main research interests are in the field of communications theory, information theory, channel and source coding with particular focus on wireless communications.